Journal of Solid State Chemistry 184 (2011) 343–350

Contents lists available at ScienceDirect

Journal of Solid State Chemistry

journal homepage: www.elsevier.com/locate/jssc

# Structural, thermodynamic and optical properties of $MgF_2$ studied from first-principles theory

K. Ramesh Babu [a], Ch. Bheema Lingam [b], S. Auluck [c], Surya P. Tewari [a,b], G. Vaitheeswaran [a,*]

[a] Advanced Centre of Research in High Energy Materials (ACRHEM), University of Hyderabad, Prof. C. R. Rao Road, Gachibowli, Andhra Pradesh, Hyderabad 500 046, India
[b] School of Physics, University of Hyderabad, Prof. C. R. Rao Road, Gachibowli, Andhra Pradesh, Hyderabad 500 046, India
[c] Department of Physics, Indian Institute of Technology Kanpur, Kanpur 208016, Uttar Pradesh, India

ARTICLE INFO

*Article history:*
Received 19 August 2010
Received in revised form
16 November 2010
Accepted 29 November 2010
Available online 7 December 2010

*Keywords:*
Band structure
Elastic constants
Thermodynamic properties
Optical properties

ABSTRACT

A detailed theoretical study of structural, electronic, elastic, thermodynamic and optical properties of rutile type $MgF_2$ has been carried out by means of first-principles Density Functional Theory (DFT) calculations using plane wave pseudo-potentials within the local density approximation and generalized-gradient approximation for the exchange and correlation functionals. The calculated ground state properties and elastic constants agree quite well with experimental values. From the calculated elastic constants we conclude that $MgF_2$ is relatively hard when compared to other alkaline-earth fluorides and ductile in nature. The thermodynamic properties such as heat capacity, entropy, free energy, phonon density of states and Debye temperatures are calculated at various temperatures from the lattice dynamical data obtained through the quasi-harmonic Debye model. From free energy and entropy it is found that the system is thermodynamically stable up to 1200 K. The imaginary part of the calculated dielectric function $\varepsilon_2(\omega)$ could reproduce the six prominent peaks which are observed in experiment. From the calculated $\varepsilon(\omega)$, other optical properties such as refractive index, reflectivity and electron energy-loss spectrum are obtained up to the photon energy range of 30 eV.



## 1. Introduction

Magnesium fluoride ($MgF_2$) is an important alkaline-earth fluoride which has attracted much attention due to its wide range of applications as an optical material for anti-reflective (AR) coatings and light polarizer [1]. Single crystal of $MgF_2$ is found to be a new optical material for semiconductor lithography because of its transmission characteristic in vacuum ultraviolet region [2]. Magnesium fluoride also known as sellaite, crystallizes in a tetragonal rutile type structure with space group $P4_2/mnm$ ($z=2$) at ambient conditions, which is same as that of the important stishovite materials $TiO_2$ and $SiO_2$. The unit cell consists of two formula units with Mg atoms fixed at symmetry centers and the fluorines have a positional degree of freedom $x(F)=y(F)$ [3]. A number of theoretical and experimental studies such as electronic structure [4–6], elastic constants [3,7], chemical bonding [8] have been carried out for $MgF_2$. An early experimental study on lattice dynamics of $MgF_2$ was reported in which the phonon spectrum of $MgF_2$ was measured by inelastic neutron scattering and the values of ionic and total polarizabilities were obtained using shell model [9]. Using semi-empirical two-body potential model, phonon dispersion relation of rutile $MgF_2$ has been calculated [10]. The high pressure behavior of alkaline-earth fluorides is of considerable interest since all the materials are ionic solids [11,12]. Among the alkaline-earth fluorides, $MgF_2$ undergoes a series of structural phase transitions from rutile $\rightarrow CaCl_2 \rightarrow PbO_2 \rightarrow PdF_2 \rightarrow$ cotunnite under high pressures around 10–36.8 GPa with an increase in cation coordination number from 6 to 9, similar to that of rutile type oxides $SiO_2$ and $GeO_2$ [13–16]. Nishidate et al., predicted through molecular dynamics calculation with the optimized MF-II potential that the rutile structure of $MgF_2$ getting transformed to cubic fluorite structure under the application of pressure of the order of 15 GPa [17]. The optical properties of $MgF_2$ are of much interest as the material is a wide band gap insulator. The opticalproperties including complex dielectric function, reflectance, refractive index and loss spectrum were determined in vacuum and extreme ultraviolet region through reflectance measurements [18,19]. By using combined tight binding and pseudo-potential method the imaginary part of the dielectric constant of $MgF_2$ was reported [20]. So far the theoretical calculations including the optical properties and thermodynamic properties like heat capacity, Debye temperature, phonon density of states of this material have been addressed relatively with less attention. Hence in the present study, efforts have been taken to shed more light on the physical properties in detail by using the plane wave pseudo-potential method. In particular we aim to obtain the elastic properties including the second order elastic constants of single crystal and thereby deduce the elastic moduli for polycrystalline material in order to determine the mechanical strength and the elastic nature of $MgF_2$. To study the nature of bonding in the material we have used Mulliken bond population and charge density distribution. The rest of the paper is organized as

* Corresponding author. Fax: +91 40 23010227.
*E-mail address:* gvsp@uohyd.ernet.in (G. Vaitheeswaran).

0022-4596/$ - see front matter © 2010 Elsevier Inc. All rights reserved.
doi:10.1016/j.jssc.2010.11.025

follows. In Section 2, we briefly describe the computational techniques while theoretical methods used are elaborated in Section 3. The results and discussion are presented in Section 4. Finally we end with a brief conclusion in Section 5.

## 2. Computational details

First-principles calculations are performed using Cambridge Series of Total Energy Package (CASTEP) based on density functional theory (DFT) with Vanderbilt-type ultrasoft pseudo-potentials [21] for electron–ion interactions to calculate the total energies and elastic properties and norm conserving pseudo-potentials as they are well suited for the calculation of thermodynamic properties using this code [22]. The exchange correlation potential of Ceperley and Alder [23] parameterized by Perdew and Zunger [24] in the local density approximation and the scheme of Perdew–Burke–Ernzerhof (PBE) [25] in generalized-gradient approximation for electron–electron interactions are used. To confirm the convergence of the calculations for the Brillouin-zone sampling, we tested the dependence of the total energy on the plane wave cut-off energy and the $k$-point mesh according to the Monkhorst-Pack grid scheme [26]. It is found that for the cut-off energy of 400 eV and $k$-point set of $5\times5\times8$, the change in total energy is minimum, so we finally choose these cut-off energy and $k$-point set for the calculation. A scissors operator of 3.97 eV in LDA and 3.92 eV in GGA is introduced to shift the conduction levels to be consistent with the measured value of the band gap [27,28]. The self-consistent convergence of the total energy is $5\times10^{-7}$ eV/atom and the maximum force on the atom is found to be $10^{-4}$ eV/Å. For the calculation of phonon density of states, the dynamical matrix elements are calculated on the $5\times5\times8$ grid of $k$-points using the linear response approach. The linear responses to ionic displacements and electric field are calculated within the density functional perturbation theory (DFPT) as implemented in CASTEP code [29,30].

## 3. Theoretical methods

### 3.1. Thermodynamic properties

Thermodynamic properties are very important, as they play an important role in understanding the thermal response of the solids. According to the standard thermodynamics, if the system is held at a fixed temperature $T$ and pressure $P$ then Gibb's free energy ($G$) of the system is expressed as

$$G(V,P,T)=E(V)+PV-TS \tag{1}$$

where $E(V)$ is the total energy, $V$ is the volume and $S$ is the entropy of the system. Since the electronic structure calculations are performed in the static approximation, i.e., at $T=0$ K and neglecting zero-point vibrational effects, the corresponding Gibb's free energy in this case becomes $G_{stat}(V,P)=E(V)+PV$, which is the enthalpy $H$ of the system. But the experimental determination of thermodynamical properties takes place at finite $T$ and therefore the vibrational effects should be considered. Hence it is necessary to include these effects in order to compare theoretical predictions with the experimental measurements to explore the thermodynamic properties. So we have chosen the quasi-harmonic Debye model [31] and according to this model the non-equilibrium Gibb's free energy function is given by

$$G^{*}(V,P,T)=E(V)+PV+A_{vib}(\Theta(V),T) \tag{2}$$

where $\Theta(V)$ is the Debye temperature, $PV$ corresponds to the constant hydrostatic pressure condition and $A_{vib}$ is the vibrational Helmholtz free energy and the corresponding expressions can be found elsewhere in [31]. The thermodynamic properties such as heat capacity ($C_v$), entropy ($S_v$) and the vibrational internal energy ($U_{vib}$) can be calculated using the following relations:

$$C_V=3nk\left[4D\left(\frac{\Theta}{T}\right)-\frac{3\frac{\Theta}{T}}{e^{\Theta/T}-1}\right] \tag{3}$$

$$S_V=nk\left[4D\left(\frac{\Theta}{T}\right)-3\ln\left(1-e^{-\Theta/T}\right)\right] \tag{4}$$

$$U_{vib}=nkT\left[\frac{9}{8}\frac{\Theta}{T}+3D\left(\frac{\Theta}{T}\right)\right] \tag{5}$$

### 3.2. Optical properties

The optical properties of matter can be described by means of the transverse dielectric function $\varepsilon(q,\omega)$ where $q$ is the momentum transfer in the photon–electron interaction and $\omega$ is the energy transfer. In the present study we have used electric-dipole approximation for the calculations, according to which $q=0$, i.e., the momentum transfer from the initial state to the final state is neglected. In general there are two contributions to $\varepsilon(\omega)$ namely intraband and interband transitions. The contribution from intraband transitions is important only for the case of metals. The interband transitions can further be split into direct and indirect transitions. The indirect interband transitions involve scattering of phonons. But the indirect transitions give only a small contribution to $\varepsilon(\omega)$ in comparison to the direct transitions [32], so we have neglected them in our calculations. The direct interband contribution to the absorptive or imaginary part of the dielectric function $\varepsilon(\omega)$ in the random phase approximation [33] without allowance for local field effects is calculated by summing all the possible transitions from the occupied and unoccupied states with fixed $k$-vector over the Brillouin zone, weighted with the appropriate transition matrix element giving the probability for the transition by

$$\varepsilon_2(\omega)=\frac{Ve^2}{2\pi\hbar m^2\omega^2}\int d^3k\ \sum|\langle\psi_C|p|\psi_V\rangle|^2\delta(E_C-E_V-\hbar\omega) \tag{6}$$

here $\psi_c$ and $\psi_v$ are the wave functions in the conduction and valence bands, $p$ is the momentum operator, $\omega$ is the photon frequency, and $\hbar$ is Planck's constant. The dispersive or real part of the dielectric function $\varepsilon(\omega)$ can be extracted from the Kramers–Kronig relation

$$\varepsilon_1(\omega)=1+\frac{2}{\pi}P\int_0^{\infty}\frac{\varepsilon_2(\omega')\omega'\,d\omega'}{(\omega')^2-(\omega)^2} \tag{7}$$

where '$P$' is the principle value of the integral. In order to calculate $\varepsilon_1(\omega)$ using Kramers–Kronig transformation, it is necessary to evaluate the absorption spectrum to high energies in order to achieve a converged result for the dispersion. So we have calculated $\varepsilon_2(\omega)$ up to 30 eV above the Fermi level. The knowledge of both the real and imaginary parts of the dielectric function allows the calculation of the important optical properties. In this paper, we present and analyze the reflectivity $R(\omega)$, energy-loss spectrum $L(\omega)$ and the refractive index $n(\omega)$ of tetragonal crystalline $MgF_2$. The reflectivity can be derived from Fresnel's formula for normal incidence assuming an orientation of the crystal surface parallel to the optical axes using the relation

$$R(\omega)=\left|\frac{(\sqrt{\varepsilon}(\omega)-1)}{(\sqrt{\varepsilon}(\omega)+1)}\right|^2 \tag{8}$$

The energy-loss spectrum $L(\omega)$ can be calculated using the following expression:

$$L(\omega)=\frac{\varepsilon_2(\omega)}{\varepsilon_1(\omega)^2+\varepsilon_2(\omega)^2} \tag{9}$$

Refractive index $n(\omega)$ can be obtained using

$$n(\omega) = \frac{1}{\sqrt{2}[\sqrt{(\varepsilon_1(\omega)^2+\varepsilon_2(\omega)^2)}+\varepsilon_1(\omega)]^{-1/2}} \quad (10)$$

## 4. Results and discussion

As a first step, we performed full structural optimization of $MgF_2$ for the unit cell and atomic positions and the crystal structure of $MgF_2$ is shown in Fig. 1. The ground state properties such as lattice constants, position of fluorine and bulk modulus are calculated and given in Table 1. The results obtained are in close agreement with the experimental values [13,34] and other theoretical calculations [14,16]. It is very well known that the LDA calculations generally underestimate the lattice constants by about 1–2% and overestimate the bulk modulus (10–12%) [35,36], whereas the GGA calculations overestimate the lattice constants (1–2%) and underestimate the bulk modulus (10–12%) [37]. We also observe a similar trend in our present calculations. Since the optical spectra are calculated from interband transitions which occur between valence and conduction bands, which in turn depends on the band gap, it would be necessary to know the electronic band structure and the magnitude of the band gap. In the present case the electronic band structure of $MgF_2$ is obtained and it is observed that the top of the valence band and bottom of the conduction band both occurs at the $\Gamma-$point, and they are separated by a gap of 6.83 eV in LDA and 6.88 eV in GGA. Therefore this is a direct band gap insulator and the magnitude of the calculated gap agrees quite well with other reported theoretical values [14]. We should note here that the nature of band gap in alkaline-earth fluorides $CaF_2$ (7.24 eV), $SrF_2$ (7.5 eV) [11] and $BaF_2$ (7.03 eV) [12] is found to be indirect, whereas in the case of $MgF_2$ it is direct. Our calculated gap of $MgF_2$ is much smaller than the experimentally reported value of 10.8 eV [38], which is due to the inherent limitation in exchange-correlation potential of LDA and GGA, and is quite common in all DFT calculations [28,35,39]. In order to obtain accurate optical transitions there is a need to reproduce the experimental band gap and this problem can be resolved by using scissor operator [40] which can produce a rigid shift of the unoccupied conduction band levels with respect to the completely occupied valence band level so that the experimentally reported band gap can be reproduced and the accurate optical transitions can be identified. So we have used scissor operator of 3.97 eV in LDA and 3.92 eV in GGA, which shifts the gap to 10.8 eV both in LDA and GGA, which is the experimental value. The scissor operator corrected band structure and density of states of $MgF_2$ is shown in Figs. 2 and 3, respectively. However one should note that scissor operator approximation is an ad hoc approximation and one needs a precise GW approximation to get the correct band structure and optical properties [41–43].

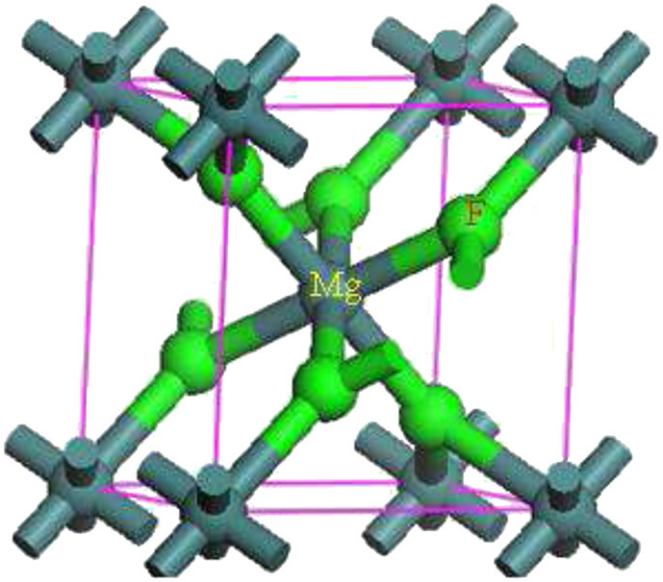


**Fig. 1.** Crystal structure of $MgF_2$.

**Table 1**
Lattice constants, position of fluorine, bulk modulus $B_0$ and band gap of $MgF_2$ together with the experimental and other theoretical values. Values in parenthesis indicate with scissor correction.

| Parameter | LDA[a] | GGA[a] | TB-LMTO[b] | VASP[c] | Expt[d] | Expt[e] |
|---|---|---|---|---|---|---|
| $a$ (Å) | 4.6028 | 4.7345 | 4.572 | 4.6912 | 4.625 | 4.621 |
| $c$ (Å) | 3.0369 | 3.1238 | 3.017 | 3.096 | 3.052 | 3.052 |
| $c/a$ | 0.6598 | 0.6598 | 0.6599 | 0.66 | 0.6599 | 0.6604 |
| $x(F)$ | 0.3026 | 0.3035 | 0.3043 | 0.3034 | 0.3027 | 0.3029 |
| $B_0$ (GPa) | 111.47 | 91.80 | 101 | 97 | $101 \pm 3$ | – |
| $E_g$ (eV) | 6.83(10.8) | 6.88(10.8) | 6.4 | – | 10.8[f] | – |

[a] Present.
[b] LDA results from Ref. [14].
[c] GGA results from Ref. [16].
[d] Ref. [13].
[e] Ref. [34].
[f] Ref. [38].

### 4.1. Chemical bonding

The nature of chemical bonding is evaluated by using Mulliken bond population analysis [44]. Bond population is an important parameter which suggests the nature of bonding between two atoms in a molecule. A positive value of the population implies that the two atoms are in bonding, whereas a negative value implies the anti-bonding. For $MgF_2$, the average Mg-F bond population is found to be $-1.72$. A charge of $-0.8|e|$ on F atom and $+1.62|e|$ on Mg atom are obtained. These results indicate a strong ionic bonding in $MgF_2$. It is well known that the ionic bond results from the electrostatic interaction of oppositely charged ions. To emphasize the coordination of Mg cation and F anion, we have plotted the electron charge density distribution of $MgF_2$ in (001) plane as shown in Fig. 4. The electron configuration of the neutral atoms of Mg and F are Mg: $1s^2 2s^2 2p^6 3s^2$, F: $1s^2 2s^2 2p^5$ respectively. The doubly charged

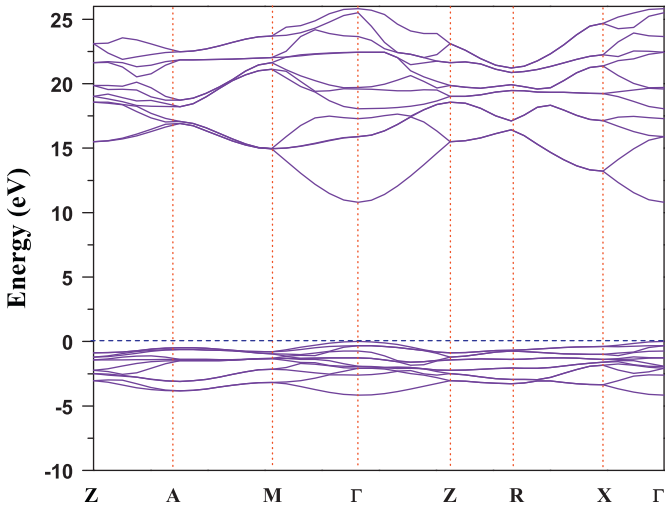


**Fig. 2.** Band structure of $MgF_2$ within LDA at theoretical equilibrium volume. A scissor operator correction of 3.97 eV is applied to shift the conduction band.

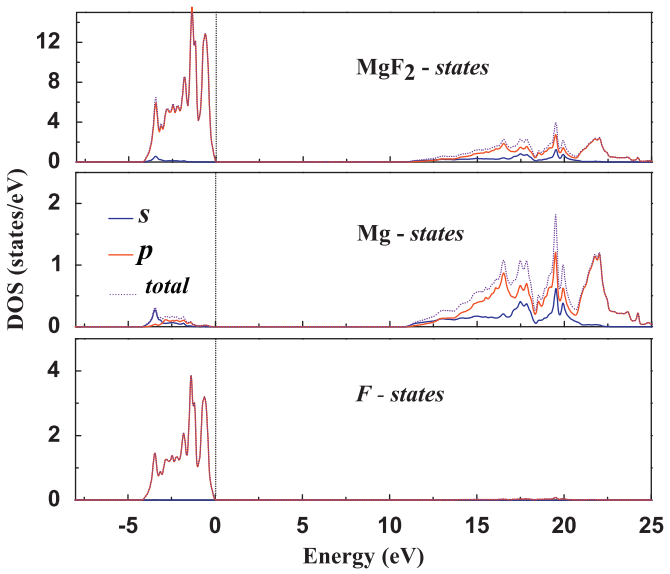


**Fig. 3.** Total and partial density of states of $MgF_2$ within LDA at theoretical equilibrium volume with a scissor operator shift.

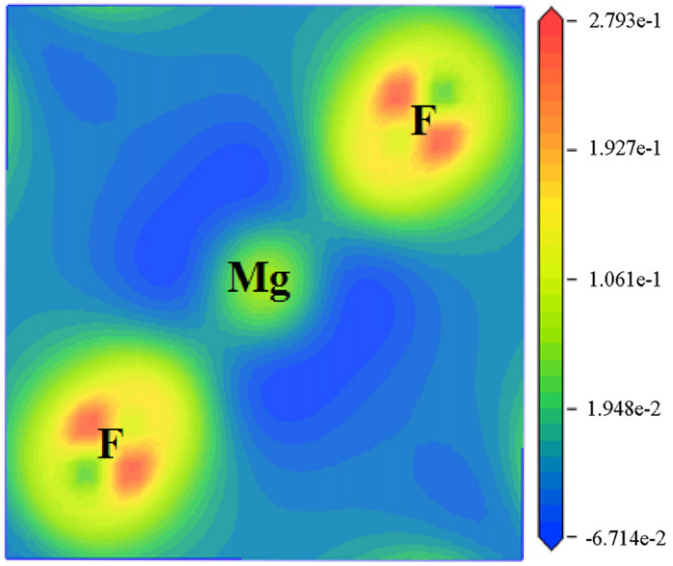


**Fig. 4.** Charge density distribution in $MgF_2$ in (001) plane within LDA. The side bar indicates the color range in the distribution.

ion of Mg and singly charged ion of F have the configurations $Mg^{2+}$: $1s^2 2s^2 2p^6$ and $F^-$: $1s^2 2s^2 2p^6$, similar to that of neon. As the inert gas atoms have closed shells, the charge distributions are spherically symmetric. Therefore we can expect that the charge distribution on each ion in $MgF_2$ crystal will have approximately spherical symmetry with some distortion near the region of contact with the neighboring ions and we can clearly observe this behavior in the charge density plot shown in Fig. 4.

### 4.2. Elastic properties

The elastic properties include elastic constants, Young's modulus, bulk modulus, shear modulus and Poisson's ratio provide information about the mechanical stability, stiffness and mechanical nature of materials to the applied stress. In particular they provide a link between the mechanical and dynamical behavior of solids. In the present study we have calculated the elastic constants for single crystal as well as polycrystalline $MgF_2$ in both LDA and GGA. Due to the tetragonal symmetry $MgF_2$ has six independent elastic constants: $C_{11}$, $C_{12}$, $C_{13}$, $C_{33}$, $C_{44}$, $C_{66}$. To calculate the elastic constants we have used the volume-conserving strains technique [45]. The obtained elastic constants are tabulated in Table 2, and are in good agreement with the experimental values and other theoretical results. The mechanical stability condition, which reflects the structural stability of materials at specific deformations, is very important. Born and Huang systematically investigated the lattice mechanical stability by expanding the internal energy of the crystal in the range of strains, in terms of elastic constants $C_{ij}$ and they found that the criterion for a mechanically stable lattice requires the elastic energy density to be a positive definite quadratic function of strain [48]. For $MgF_2$ it is found that all the elastic constants are positive and obey Born's criteria for mechanical stability of tetragonal crystals given by $C_{11}>0$, $C_{33}>0$, $C_{44}>0$, $C_{66}>0$, $(C_{11}-C_{12})>0$, $(C_{11}+C_{33}-2C_{13})>0$ and $[2(C_{11}+C_{12})+C_{33}+4C_{13}]>0$. The anisotropy factor $A=2C_{44}/(C_{11}-C_{12})$ of $MgF_2$ is 2.26 in LDA and 2.03 in GGA. This reveals that $MgF_2$ is anisotropic, because the value $A=1$ represents complete elastic isotropy, while values smaller or greater than 1 measures the degree of elastic anisotropy. The obtained elastic constants allow us to obtain the macroscopic mechanical properties of $MgF_2$, namely bulk moduli ($B$) and shear moduli ($G$) via two approximations: Voigt ($V$) and Reuss ($R$) in the following forms:

$$B_V = \tfrac{1}{9}[2(C_{11}+C_{12})+C_{33}+4C_{13}] \tag{11}$$

$$G_V = \tfrac{1}{30}(L+3C_{11}-3C_{12}+12C_{44}+6C_{66}) \tag{12}$$

$$B_R = \frac{C^2}{L}, \quad G_R = 15\left[18\frac{B_V}{C^2}+\frac{6}{(C_{11}-C_{12})}+\frac{6}{C_{44}}+\frac{3}{C_{66}}\right]^{-1} \tag{13}$$

where $L=C_{11}+C_{12}+2C_{33}-4C_{13}$ and $C^2=(C_{11}+C_{12})C_{33}-2C_{13}^2$. The results obtained are summarized in Table 3. By using the predicted

**Table 2**
Single-crystal elastic constants ($C_{ij}$ in GPa), bulk moduli ($B$ in GPa), shear moduli ($G$ in GPa) and anisotropy factor ($A$) of $MgF_2$ together with the experimental and other theoretical values.

| Parameter | LDA | GGA | HF-LCAO[a] | VASP (GGA)[b] | Expt[c] | Expt[d] |
|---|---|---|---|---|---|---|
| $C_{11}$ | 145.68 | 122.76 | 155.3 | 130.80 | 140.81 | 142.7 |
| $C_{12}$ | 101.94 | 75.73 | 90.7 | 83.80 | 90.03 | 92.2 |
| $C_{13}$ | 75.63 | 57.74 | 55.6 | 59.25 | 64.17 | 64.1 |
| $C_{33}$ | 208.21 | 178.99 | 219.3 | 193.60 | 204.90 | 204 |
| $C_{44}$ | 49.64 | 47.74 | 68.2 | 52.70 | 56.64 | 56.7 |
| $C_{66}$ | 102.52 | 83.05 | 104.1 | 89.30 | 95.60 | 93.5 |
| $B_V$ | 111.7 | 89.65 | – | – | – | |
| $B_R$ | 110.96 | 88.66 | – | – | – | |
| $G_V$ | 56.78 | 51.25 | – | – | – | |
| $G_R$ | 44.52 | 43.46 | – | – | – | |
| $A$ | 2.26 | 2.03 | – | – | – | |
| $A_B$(%) | 0.36 | 0.55 | – | – | – | |
| $A_G$(%) | 12.1 | 8.22 | – | – | – | |

[a] Ref. [3].
[b] Ref. [16].
[c] Ref. [46].
[d] Ref. [47].

**Table 3**
Polycrystaline aggregate properties of bulk moduli ($B_{VRH}$, in GPa), compressibility ($\beta_{VRH}$, in $GPa^{-1}$), shear moduli ($G_{VRH}$, in GPa), Young's moduli ($E_{VRH}$, in GPa) and Poisson's ratio ($\sigma$) in Voigt–Reuss–Hill approximation.

| $MgF_2$ | $B_{VRH}$ | $\beta_{VRH}$ | $G_{VRH}$ | $E_{VRH}$ | $\sigma$ |
|---|---|---|---|---|---|
| LDA | 111.37 | 0.0089 | 50.65 | 131.94 | 0.3 |
| GGA | 89.15 | 0.0112 | 47.35 | 120.68 | 0.28 |

$C_{ij}$'s of $MgF_2$, we find the polycrystalline aggregate properties such as bulk moduli ($B$), which measures the resistance of a material against volume change under hydrostatic pressure, and shear modulus ($G$), which represents the resistance to shape change caused by shearing force in terms of Voigt–Reuss–Hill approach [49]. In this approach according to Hill, the Voigt and Reuss averages are limits and the actual effective moduli for polycrystals can be approximated by the arithmetic mean of these two limits. Then, one can calculate the average compressibility ($\beta_{VRH} = 1/B_{VRH}$), Young's modulus ($Y_{VRH} = 9G_{VRH}B_{VRH}/(3B_{VRH} + G_{VRH})$), which reflects the resistance of material against uniaxial tensions and also Poisson's ratio $\sigma = 1/2[(B_{VRH} - (2/3)G_{VRH}/(B_{VRH} + (1/3)G_{VRH})]$, which generally indicates the stability of the crystal against shear and takes the value between $-1$ and 0.5 which are the lower and upper bounds. The lower bound indicates where the material does not change its shape and the upper bound resembles the case where the volume remains unchanged. All these parameters are listed in Table 3. From our results we can see that for polycrystalline $MgF_2$, $B_{VRH} > G_{VRH}$ in both LDA and GGA which implies that the parameter limiting the mechanical stability of $MgF_2$ is the shear modulus $G_{VRH}$. On the other hand the bulk moduli for $MgF_2$ is large ($> 100$ GPa) and also for example greater than the bulk moduli for other alkaline-earth fluorides; $CaF_2$ (84.1 GPa) [50], $SrF_2$ (69 GPa) [51], $BaF_2$ (57 GPa) [52]. Thus, when compared with other alkaline-earth fluorides $MgF_2$ is a relatively hard material. To know the ductile–brittle nature of $MgF_2$ we have used Pugh's criterion [53], according to which the critical value of $B/G$ ratio that separates the ductile and brittle nature of a material is found to be 1.75. In our case this value is found to be 2.19 in LDA and 1.88 in GGA, respectively. This means that $MgF_2$ is a ductile material and this behavior can be connected to the elastic anisotropy which is an important factor in estimating the possibility of inducing microcracks in the material. We have estimated the elastic anisotropy ($A_B$, in percent) in terms of compressibility and shear for polycrystalline materials as $A_B = (B_V - B_R)/(B_V + B_R)$ and $A_G = (G_V - G_R)/(G_V + G_R)$ [54]. The farther values of $A_B$ and $A_G$ from zero indicate larger anisotropy of material. For isotropic materials $A_B = A_G = 0$. The calculated values for $MgF_2$ are: $A_B$ (0.363% in LDA and 0.55% in GGA) and $A_G$ (12.1% in LDA and 8.22% in GGA), also shown in Table 2, indicate that the material is anisotropic in nature. The values of the Poisson's ratio $\sigma$ for covalent materials are small ($\sigma = 0.1$), whereas for ionic materials a typical value of $\sigma$ is 0.25 [55]. In our case the value of $\sigma$ for $MgF_2$ is about 0.304 in LDA and 0.276 in GGA, i.e., a considerable ionic contribution to intra-atomic bonding can be assumed. For covalent and ionic materials, the typical relations between bulk and shear moduli are $G \approx 1.1B$ and $G \approx 0.6B$, respectively [55]. In our case the calculated values of $MgF_2$ are $G_{VRH} = 0.45B_{VRH}$ in LDA and $G_{VRH} = 0.53B_{VRH}$ in GGA, which also indicates that the ionic bonding is predominant in $MgF_2$. This may also be clearly seen on the electron density map for $MgF_2$ shown in Fig. 4.

### 4.3. Thermodynamic properties

Free energy, heat capacity, entropy and phonon density of states are important thermodynamic properties of solids. Following the theory of quasi-harmonic Debye model outlined in Section 3.1, in which the phonons are harmonic but they are volume dependent, we have calculated the thermodynamic properties of $MgF_2$. The total phonon density of states of $MgF_2$ are obtained and shown in Fig. 5(a). From the phonon density of states it can be seen that the high frequency modes are dominated by the F atoms due to their low masses, whereas the low frequency modes are essentially dominated by Mg atoms. We find that the calculated phonon density of states spectra is in good agreement with the earlier reported spectra in [10]. The calculated total phonon DOS is used to evaluate the temperature dependence of thermodynamic properties of $MgF_2$. Usually, the quasi-harmonic approximation is not valid when the temperature is close to the melting point of the lattice [56]. So we have used a truncated temperature range from 0 to 1200 K which is below the melting point of $MgF_2$ (1534 K). The contributions from the lattice vibrations to the heat capacity are shown in Fig. 5(b). The obtained temperature dependent heat capacity follows the Debye model and approaches the Debye $T^3$ law at low temperatures ($< 50$ K) and reaches the Dulong–Petit limit at high temperatures ($> 600$ K). Our calculated heat capacity is in good agreement with the experimental results of Todd [57] at low temperatures of below 150 K, whereas above this temperature there is a discrepancy in the calculated and experimental value of the heat capacity. The probable reason for this discrepancy is that the material might have strong anharmonicity above this temperature and this behavior increases with increase in temperature. Because the used quasi-harmonic approximation (QHA) accounts only partially the effects of anharmonicity, through the volume dependence of the phonons [58], we could only get the good agreement between the calculated and experimental heat capacity at low temperatures ($< 150$ K) rather than at high temperatures ($> 150$ K). The Debye temperature, the highest temperature that can be achieved due to a single normal mode, of a solid is a material dependent parameter that is involved in all physical phenomena where the lattice vibrations play an important role, such as thermal conductivity, super conductivity, phonon spectra, melting point and others. Since the Debye temperature shows strong temperature dependence, we calculated this dependence up to the temperature range of 1200 K and shown in Fig. 5(c). The calculated Debye temperature increases with increase in temperature and shows a large variation from 200 to 1200 K in the high temperature limit. The calculated vibrational entropy of $MgF_2$ is shown in Fig. 5(d). As the temperature increases the vibrational contribution to the entropy increases and therefore the entropy increases with temperature. It is well known that, as the temperature rises the contribution of phonons become more and more important and one can calculate the free energy $F = U - TS$, where $U$ the vibrational internal energy given in Eq. (5) contains the static energy and the phonon contribution and $S$ is the entropy which is entirely due to phonons and it is shown in Fig. 5(e). The calculated free energy ($F = U - TS$) of $MgF_2$ decreases with the increase in temperature. This behavior is due to the fact that both vibrational internal energy $U$ and entropy $S$ increases with temperature and this leads to the decrease in free energy. From the study of free energy we conclude that the system is thermodynamically stable below 1200 K.

### 4.4. Optical properties

Now we try to shed more light on the optical properties using the calculated scissor operator corrected band structure. The fine structure of the energy distribution of the electron states in the valence and conduction bands can be obtained by the knowledge of the optical functions. The interband optical functions are calculated by using the expressions as stated in Section 3.2. For the calculation we have taken the electric field vector as an average over the plane perpendicular to the polarization direction of [100]. The absorptive part $\varepsilon_2(\omega)$ and the dispersive part $\varepsilon_1(\omega)$ of the complex dielectric function $\varepsilon(\omega)$ as a function of the photon energy are shown in Figs. 6(a) and (b) respectively, where the dotted lines represent the experimental data. The assignments of the critical peaks in the optical spectra of $\varepsilon_2(\omega)$ in Fig. 6(a) are as follows. Peak A at 10.89 eV originates from the transition F $2p$ (at $-0.04$ eV) $\rightarrow$ Mg $3s$ (at 10.85 eV) at $\Gamma$–point. The peak B at 12.53 eV arises from the transition F $2p$ (at $-1.68$ eV) $\rightarrow$ Mg $3s$ (at 10.85 eV) at $\Gamma$–point. The peak C at 13.77 eV is due to the transition F $2p$ (at $-0.50$ eV) $\rightarrow$ Mg $3s$ (at 13.27 eV) at $X$-point. The peak D at 15.37 eV probably arises from the transition F $2p$ (at $-0.57$ eV) $\rightarrow$ Mg $3s$ (at 14.80 eV) at $M$-point. Peak E at 16.84 eV is due to the transition F $2p$ (at $-0.31$ eV)

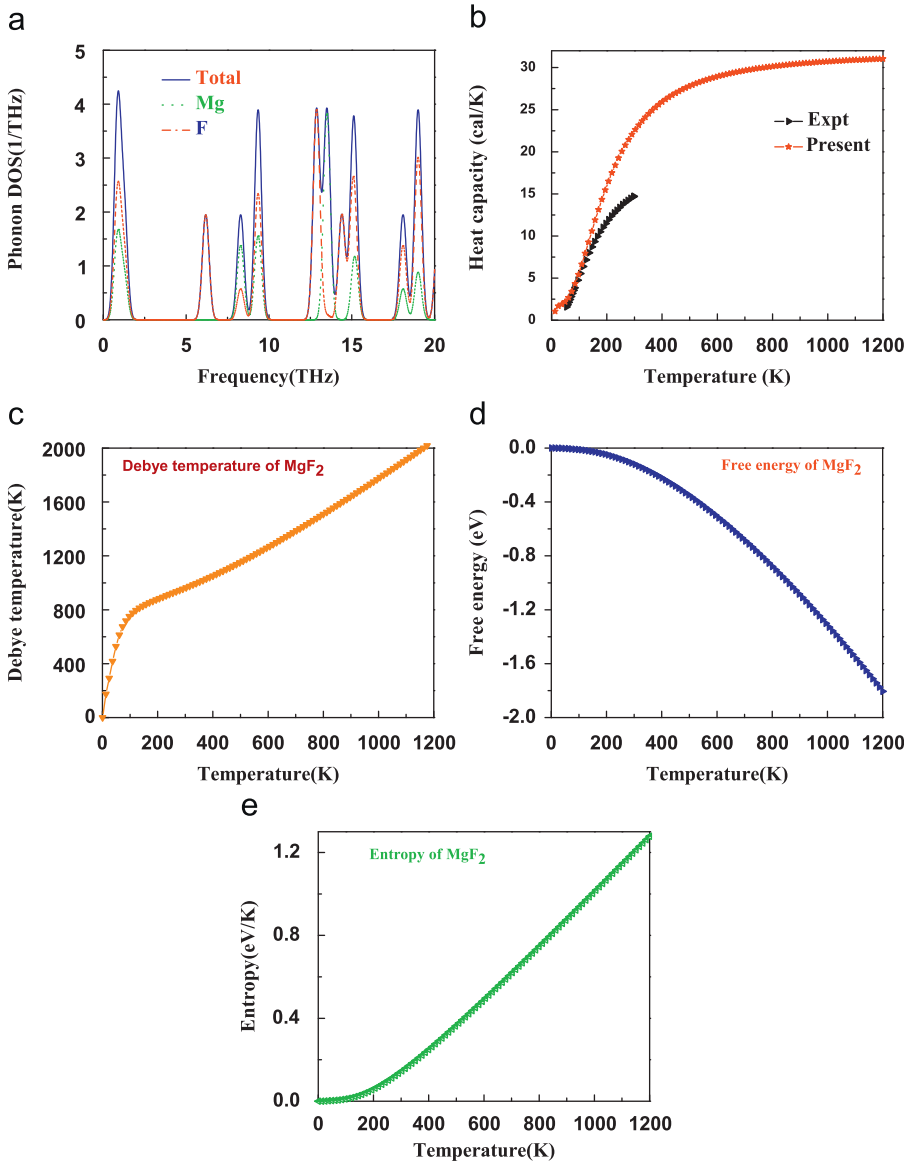


**Fig. 5.** Thermodynamic properties of $MgF_2$ calculated within LDA at the theoretical equilibrium volume.

→ Mg 3*s* (at 16.53 eV) at *A*-point. The highest peak, F, at 22.01 eV may be due to the transition F 2*p* (at −3.35 eV) → Mg 3*s* (at 18.66 eV) at *Z*-point. It should be note that all the optical transitions are mainly from F '*p*' states to the '*s*' states of Mg, this is because F 2*p* states dominate up to −5 eV in the valence band and Mg 3*s* states are dominate up to 22 eV in the conduction band. Our calculated $\varepsilon_2(\omega)$ is in good agreement with the experimental result of William et al. [18] where the peaks A (11.75 eV), B (13.23 eV), C (14.30 eV), D (15.32eV), E (17.20 eV) and F (20.93 eV) observed respectively. The $\varepsilon_1(\omega)$ is also in good agreement with the experimental data [18]. A good measure of the consistency of our calculations can be inferred from the fact that the calculated $\varepsilon_1(0)$ is 1.79 is in good comparison with the experimental value of 1.90 [18]. The calculated refractive index $n(\omega)$ is shown in Fig 6(c) along with the experimental data [18]. The static refractive index $n(0)$ is found to have the value of 1.33 which is in good agreement with the experimental value of 1.38 [18] and 1.36 [59]. The refractive index reaches a maximum value of 1.61 at 9.8 eV, whereas the experimental value is 2.24 at 11.55 eV. We should note here that the experimental first peak in all the observed optical spectra is more intense compared to the theoretical peak. The discrepancy may be due to the inadequacy of the exchange-correlation functionals in DFT as regards in reproducing the experimental results. The reflectivity $R(\omega)$ of $MgF_2$ is shown in Fig. 6(d). By carefully analyzing the reflection spectrum we propose that $MgF_2$ has the potential to be used as anti-reflection coating material in the energy range of nearly up to 3 eV i.e., in the mid visible region and it is a good reflecting material for the vacuum ultraviolet radiation as the spectrum shows large peak around 26 eV which is also in consistent with the experimental peak around 25 eV. The energy-loss function which is the imaginary part of the reciprocal of the complex dielectric function is also obtained and shown in Fig. 6(e). It is an important optical parameter, indicating the energy loss of a fast electron traversing in the material. The peaks represent the characteristic behaviors associated with the plasma oscillations and the corresponding frequencies are the so-called plasma frequencies. The peaks of $L(\omega)$ correspond to the trailing edges in the reflection spectra and is observed at around 26 eV corresponding to the abrupt reduction of $R(\omega)$. This is in good agreement with the experimentally reported value of 24.5 eV [18].

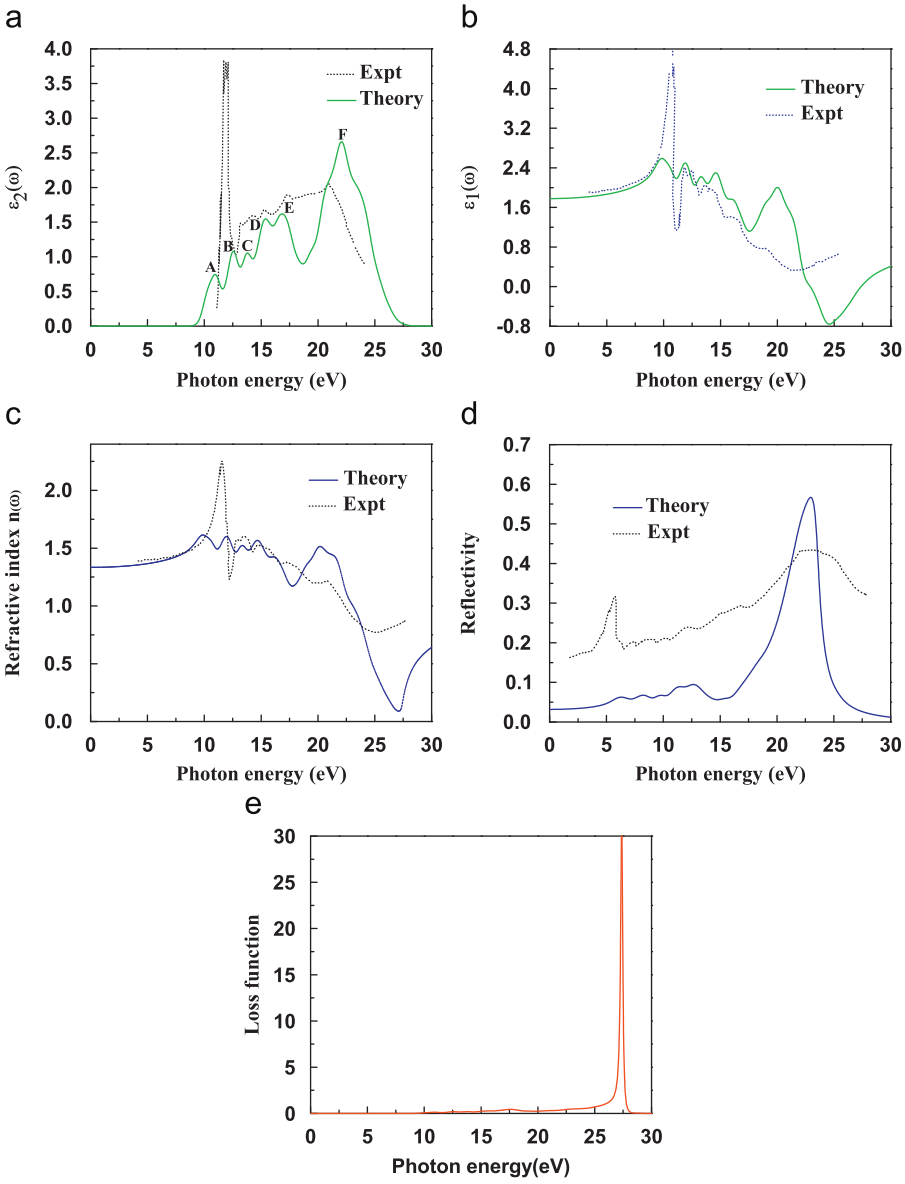


**Fig. 6.** Optical properties of $MgF_2$ calculated within LDA at theoretical equilibrium volume (the $\varepsilon_2(\omega)$ corresponds to the scissor shift of 3.97 eV).

## 5. Conclusions

Full structural optimization of the rutile type $MgF_2$ has been carried out to obtain the equilibrium structural properties like cell constants, atomic position and bulk modulus of the system which are in close agreement with the experimental results. The calculations show that $MgF_2$ has a direct band gap of 6.83 eV in LDA and 6.88 eV in GGA with a scissors operator correction of 3.97 eV in LDA and 3.92 eV in GGA to compare with the experimental band gap of 10.8 eV. The Mulliken bond population analysis and the charge density distribution plots indicate that the material is ionic. We have calculated the elastic properties for single and polycrystalline $MgF_2$. Our analysis shows that $MgF_2$ is a mechanically stable anisotropic material, the only parameter limiting the mechanical stability is the shear modulus. In addition, $MgF_2$ is relatively hard material with less compressibility compared to other alkaline-earth fluorides, which also exhibits ductile behavior and with a high ionic contribution to intra-atomic bonding. We have investigated the basic thermodynamic properties using the quasi-harmonic Debye model and is seen that the predicted heat capacity $C_v$ is close to the Dulong–Petit limit, which is common to all solids at high temperatures. The temperature dependent entropy and free energy of $MgF_2$ show that it is thermodynamically stable below 1200 K. Finally we have calculated the optical properties of $MgF_2$ and found that they are in good agreement with experiment and the material can be used as an anti-reflecting coating material in the energy range of 2–4 eV and also can be used as reflective coating material in the regime of vacuum ultraviolet region.

## Acknowledgments

K.R.B. and Ch.B.L. thank Dr. V. Kanchana for valuable discussions and also thank Prof. C.S. Sunandana for critical reading of the manuscript. K.R.B. would like to thank DRDO through ACRHEM for financial support. The authors acknowledge CMSD University of Hyderabad for the computational facilities.

## References


[1] O. Duyar, H.Z. Durusoy, Turk. J. Phys. 28 (2004) 139–144.
[2] Y. Kitamura, N. Miyazaki, T. Mabuchi, T. Nawata, J. Cryst. Growth 311 (2009) 3954–3962.
[3] M. Catti, A. Pavese, R. Dovesi, C. Roetti, M. Causa, Phys. Rev. B 44 (1991) 3509–3517.
[4] R.C. Chaney, J. Phys. C: Solid State Phys. 13 (1980) 5691–5699.
[5] A.B. Sobolev, I.F. Bikmetov, P.V. Lushnikov, Yu.S. Tipenko, M.V. Nikanovich, A.A. Stavrov, A.P. Shkadarevich, Spektroskopii 54 (6) (1991) 986–990.
[6] J. Robertson, J. Phys. C: Solid State Phys. 12 (1979) 4767.
[7] J. Chen, L.L. Boyer, H. Krakauer, M.J. Mehl, Phys. Rev. B 37 (1988) 3295.
[8] E. Fransico, J.M. Recio, M.A. Blanco, A. Martn Pends, A. Costales, J. Phys. Chem. A 102 (9) (1998) 1595–1601.
[9] R. Almairac, C. Benoit, J. Phys. C: Solid State Phys. 7 (1974) 2614.
[10] H. Kim, Met. Mater. Int. 7 (1) (2001) 33–37.
[11] V. Kanchana, G. Vaitheeswaran, M. Rajagopalan, Physica B 328 (2003) 283–290.
[12] V. Kanchana, G. Vaitheeswaran, M. Rajagopalan, J. Alloys Compds. 359 (2003) 66–72.
[13] J. Haines, J.M. Leger, F. Gorelli, D.D. Klug, J.S. Tse, Z.Q. Li, Phys. Rev. B 64 (2001) 134110.
[14] V. Kanchana, G. Vaitheeswaran, M. Rajagopalan, J. Alloys Compds. 352 (2003) 60–65.
[15] K. Kusuba, T. Kikegawa, Solid State Commun. 148 (2008) 440–443.
[16] L. Zhang, Y. Wang, T. Cui, Y. Ma, G. Zou, Solid State Commun. (c) 145 (2008) 283–287.
[17] K. Nishidate, M. Baba, T. Sato, K. Nishikawa, Phys. Rev. B 52 (5) (1995) 3170–3176.
[18] M.W. Williams, R.A. Macrae, E.T. Arakawa, J. Appl. Phys. 38 (4) (1967) 1701–1705.
[19] W.F. Hanson, E.T. Arakawa, M.W. Williams, J. Appl. Phys. 43 (4) (1972) 1661–1665.
[20] C. Jouanin, J.P. Albert, C. Gout, Le Journal De Physique Tome 37 (1976) 595–602.
[21] D. Vanderbilt, Phys. Rev. B 41 (1990) 7892.
[22] M.D. Segall, P.L.D. Lindan, M.J. Probert, C.J. Pickard, P.J. Hasnip, S.J. Clark, M.C. Payne, J. Phys. Condens. Matter 14 (2002) 2717.
[23] D.M. Ceperley, B.J. Alder, Phys. Rev. Lett. 45 (1980) 566.
[24] J.P. Perdew, A. Zunger, Phys. Rev. B 23 (1981) 5048.
[25] J.P. Perdew, K. Burke, M. Ernzerhof, Phys. Rev. Lett. 77 (1996) 3865.
[26] H.J. Monkhorst, J.D. Pack, Phys. Rev. B 13 (1976) 5188.
[27] O. Gunnarsson, K. Schonhammer, Phys. Rev. Lett. 56 (18) (1986) 1968–1971.
[28] V. Fiorentini, A. Baldereschi, Phys. Rev. B 51 (1995) 17196–17198.
[29] X. Gonze, Phys. Rev. B 55 (1997) 10337–10354.
[30] K. Refson, P.R. Tulip, S.J. Clark, Phys. Rev. B 73 (2006) 155114.
[31] M.A. Blanco, E. Francisco, V. Luana, Comput. Phys. Commun. 158 (2004) 57–72.
[32] N.V. Smith, Phys. Rev. B 3 (1971) 1862.
[33] H. Ehrenreich, M.H. Cohen, Phys. Rev. 115 (1959) 786.
[34] W.H. Baur, Acta Crystallogr. B 32 (1976) 2200.
[35] R.O. Jones, O. Gunnarsson, Rev. Mod. Phys. 61 (1989) 689–746.
[36] S.B. Trickey, Int. J. Quantum Chem. 61 (1997) 641–646.
[37] J.P. Perdew, J.A. Chevary, S.H. Vosko, K.A. Jackson, M.R. Pederson, D.J. Singh, C. Fiolhais, Phys. Rev. B 46 (1992) 6671–6687.
[38] 〈www.Almazoptics.com〉.
[39] J.P. Perdew, M. Levy, Phys. Rev. Lett. 51 (1983) 1884–1887.
[40] F.M. Hossain, L. Sheppard, J. Nowotny, G.E. Murch, J. Phys. Chem. Solids 69 (2008) 1820–1828.
[41] M.S. Hybertsen, S.G. Louie, Phys. Rev. B 34 (1986) 5390–5413.
[42] V. Kanchana, G. Vaitheeswaran, P. Souvatzis, O. Eriksson, S. Lebègue, J. Phys. Condens. Matter 22 (2010) 445402.
[43] S. Lebègue, B. Arnaud, M. Alouani, P.E. Blöechl, Phys. Rev. B 67 (2003) 155208.
[44] R.S. Mulliken, J. Chem. Phys. 23 (1955) 1833.
[45] M.J. Mehl, J.E. Osburn, D.A. Papaconstantopoulus, B.M. Klein, Phys. Rev. B 41 (1990) 10311.
[46] D. Gerlich, S. Hart, D. Whittal, Phys. Rev. B 29 (1984) 2142.
[47] G.F. Davis, Earth Planet. Sci. Lett. 34 (1977) 300–306.
[48] M. Born, K. Huang, Dynamical Theory of Crystal Lattices, Oxford University Press, Oxford, 1998.
[49] R. Hill, Proc. Phys. Soc. London A 65 (1952) 349.
[50] C. Wang, D.E. Schuele, J. Phys. Chem. Solids 29 (1968) 1309.
[51] G.A. Samara, Phys. Rev. B 13 (1976) 4529.
[52] J.M. Leger, J. Haines, A. Atouf, O. Schulte, S. Hull, Phys. Rev. B 52 (1995) 13247.
[53] S.F. Pugh, Philos. Mag. 45 (1954) 823.
[54] S.L. Shang, G. Sheng, Y. Wang, L.Q. Chen, Z.K. Liu, Phys. Rev. B 80 (2009) 052102.
[55] J. Haines, J.M. Leger, G. Bocquillon, Ann. Rev. Mater. Res. 31 (2001) 1.
[56] S. Baroni, S. de Gironcoli, A.D. Corso, Rev. Mod. Phys. 73 (2001) 515.
[57] S.S. Todd, J. Am. Chem. Soc. 71 (1949) 4115.
[58] S. Baroni, P. Giannozzi, E. Isaev, Rev. Mineral. GeoChem. 71 (2009) 1–19.
[59] J.M. Siqueiros, R. Machorro, L.E. Regalado, Appl. Opt. 27 (1988) 2549.